A 3.9GHz/63.6% FBW Multi-Mode Filtering Power Divider Using Self-Packaged SISL

Jian-Kang Xiao, *Member, IEEE*, Xiao-Yun Yang, and Xiao-Fang Li

***Abstract*—In this brief, a self-packaged substrate integrated suspended line filtering power divider with wideband and high frequency selectivity by using coupled-line termination added multi-mode resonator has been developed, and has been demonstrated by experiment. Three transmission zeros have been realized due to the coupled-line termination loaded stepped impedance resonator and multi-mode resonator, which improve the frequency selectivity and out-of-band suppression importantly. The wideband filtering power divider has a measured center frequency of 3.9GHz, a fractional bandwidth of 63.6%, an insertion loss of 0.74dB, an in-band isolation (S_{23}) of no less than 18.3dB, and an out-of-band rejection of more than 40dB.**

***Index Terms*—Filtering power divider, multi-mode resonator, wideband, self-packaging, suspended line.**

I. Introduction

WILKINSON power dividers have been widely used in amplifiers, mixers, and antenna feeding networks, *et al.* With the development of 5G communication and MIMO (multi-input and multi-output) technology, more power dividers would be desired. The traditional Wilkinson power divider has poor out-of-band rejection, fortunately, filtering power divider (FPD) [1]–[14] which integrates a bandpass filter and a power divider overcomes the drawback effectively.

Wideband communication systems which have advantage of accommodating more information capacity desire wideband components such as wideband FPDs. A wideband filtering power divider can be designed by a wideband bandpass filter cascading a power divider, or inserting a wideband bandpass filter into a power divider, for example, substituting the impedance transformer of the Wilkinson power divider by a wideband bandpass filter. Multi-mode resonator is the most effective method for implementing a wideband bandpass filter. Reference [1] proposed a filtering power divider by using multi-mode resonators, however, the bandwidth is very limited. In [9], tri-mode resonator is used simultaneous realizing of wideband power division and port-to-port isolation. Other methods such as three coupled lines also have been used for implementing wideband filtering power dividers [7], [12]. In recent years, wideband FPD with equal-ripple level [10], and dual-wideband FPD [13] also have been developed, and multiple resistors are used for improving the FPD isolation [8]. It is noted that all of these designs are microstrip circuits.

The traditional suspended line with metal mechanical housing has been successfully used for implementing filters [15], amplifiers [16], mixers [17], and oscillators [18], *et al*. However, the disadvantages of bulky circuit size, heavy weight and mechanical mounting prevent the development of this kind of circuit. With the circuit development for integration and multi-function, three dimensional multi-layer circuits have been paid more and more attention. Multi-layer substrate integrated suspended line (SISL) [19] inherits the advantages of the traditional suspended line, but overcomes its shortcomings.

This brief aims to develop new self-packaged multi-layer suspended multi-mode wideband filtering power divider with bandpass filter response by using SISL technology. The proposed wideband FPD in this brief has a simple structure composing of a coupled-line terminal loading quad-mode resonator and stepped-impedance resonator (SIR). Three transmission zeros (TZs) and adjustable bandwidth is implemented. The proposed FPD has been fabricated by common PCB technique layer by layer, and then assembled together by the rivets. Experiments have been performed and the design has been demonstrated with center frequency of 3.9GHz, passband insertion loss of no more than 0.74dB, in-band/out-of-band isolation of no less than 18.3/36.5dB, out-of-band rejection of more than 40dB, and multiple TZs.

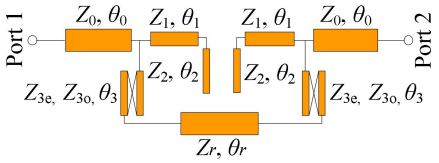

Fig. 1. Transmission line circuit model of the multi-mode wideband bandpass filter.

II. Wideband Filtering Power Divider Design

A. Multi-Mode Wideband Bandpass Filter Design

A wideband bandpass filter is designed by using coupled-line terminal loading multi-mode resonator and a pair of open circuited SIR, as is shown in Fig. 1. The coupled-line terminal loading multi-mode resonator is used to realize a wideband response, while the loading open circuited SIR is used for introducing additional transmission zeros. The coupled-line terminal loading multi-mode resonator is shown in Fig. 2, where the multi-mode resonator and the coupled-line terminal loading structure are plotted in Figs. 2(a) and (b), respectively. Where Z_{0e} and Z_{0o} are the characteristic impedances of the even-mode and odd-mode of the coupled-line, respectively, Z_r

Manuscript received November 16, 2020; revised December 21, 2020; accepted December 27, 2020. Date of publication December 30, 2020; date of current version May 27, 2021. This work was supported in part by the National Natural Science Foundation of China under Grant 61871458. This brief was recommended by Associate Editor X. Wang. *(Corresponding author: Jian-Kang Xiao.)*

The authors are with the School of Electro-Mechanical Engineering, Xidian University, Xi'an 710071, China (e-mail: jkxiao@xidian.edu.cn).

Color versions of one or more figures in this article are available at https://doi.org/10.1109/TCSII.2020.3048108.

Digital Object Identifier 10.1109/TCSII.2020.3048108

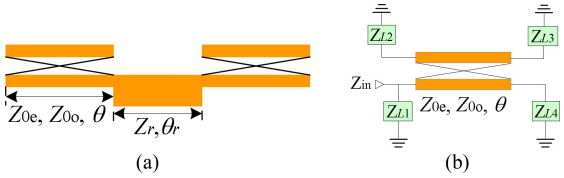

Fig. 2. Coupled-line terminal loading multi-mode resonator. (a) Multi-mode resonator structure. (b) Coupled-line terminal loading structure.

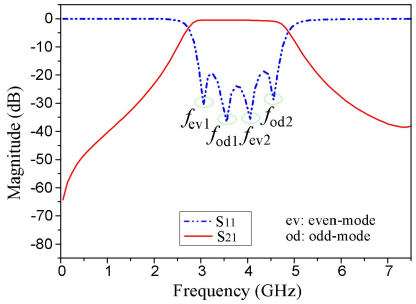

Fig. 3. Circuit simulation result of the coupled-line terminal loading multi-mode resonator. $Z_{0e} = 176\Omega$, $Z_{0o} = 79\Omega$, $\theta = 89°$, $k = 0.38$ (coupling coefficient of the coupled line), $Z_r = 42\Omega$, and $\theta_r = 85°$.

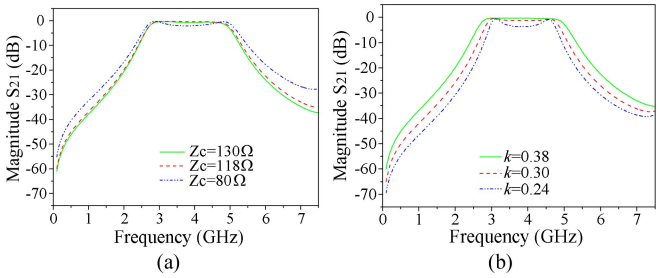

Fig. 4. Simulation result of S_{21} variations versus Z_c and k for the coupled-line terminal loading multi-mode resonator, $Z_r = 42\Omega$, and $\theta_r = 85°$. (a) S_{21} versus Z_c variation, $k = 0.38$. (b) S_{21} versus k variation, $Z_c = 118\Omega$.

is the characteristic impedance of the multi-mode resonator, and Z_{Li} $(i = 1, 2, 3, 4)$ is the terminal load of the coupled-line.

The simulated result of the coupled-line terminal loading multi-mode resonator by using ADS is shown in Fig. 3, which indicates that four resonances (four resonant modes) f_{ev1}, f_{od1}, f_{ev2}, and f_{od2} compose a wide passband, and each resonant mode introduces a transmission pole, and the resonator bandwidth is determined by f_{od2}–f_{ev1}. Circuit simulation result of S_{21} variations versus Z_c and k are plotted in Figs. 4(a) and (b), respectively, here Z_c and k are the characteristic impedance and coupling coefficient of the coupled line, respectively, and $Z_c = \sqrt{Z_{0e}Z_{0o}}$. It can be seen that resonator bandwidth increases with Z_c decreasing, as shown in Fig. 4(a); while bandwidth decreases with coupling coefficient k decreasing, as shown in Fig. 4(b), which means that weak coupling brings decreased bandwidth, and when k=0.38, the even-mode and odd-mode characteristic impedances of the coupled-line can be achieved as $Z_{0e} = 176\Omega$, and $Z_{0o} = 79\Omega$, respectively; when $k = 0.30$, it can be obtained that $Z_{0e} = 160\Omega$, and $Z_{0o} = 86.8\Omega$; while when k=0.24, it is achieved that $Z_{0e} = 150\Omega$, and $Z_{0o} = 92.6\Omega$. The circuit substrate permittivity is 2.2, and thickness is 0.254mm.

Even-mode and odd-mode equivalent circuits of the bandpass filter are shown in Figs. 5(a) and (b), respectively. The

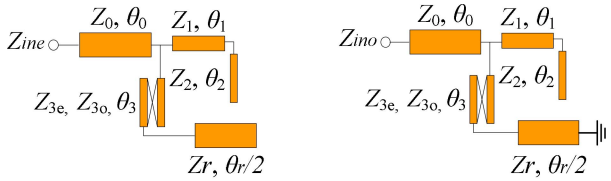

Fig. 5. Even-mode and odd-mode equivalent circuits of the proposed bandpass filter. (a) Even-mode equivalent circuit. (b) Odd-mode equivalent circuit.

input impedance of the even-mode and the odd-mode equivalent circuits can be obtained by the coupled-line terminal loading theory. The impedance ratio is defined as

$$K = Z_1/Z_2 \tag{1}$$

The input impedance of the Even-mode circuit can be expressed as

$$Z_{ine} = Z_{in} \tag{2}$$

with $Z_{L1} = jZ_1\frac{K\tan\theta_1 - \cot\theta_2}{K + \cot\theta_2\tan\theta_1}$, $Z_{L2} = \infty$, $Z_{L4} = \infty$, and $Z_{L3} = -jZ_r\cot\frac{\theta_r}{2}$.

While the input impedance of the odd-mode circuit can be expressed as

$$Z_{ino} = Z_{in} \tag{3}$$

with $Z_{L1} = jZ_1\frac{K\tan\theta_1 - \cot\theta_2}{K + \cot\theta_2\tan\theta_1}$, $Z_{L2} = \infty$, $Z_{L4} = \infty$, and $Z_{L3} = jZ_r\tan\frac{\theta_r}{2}$.

According to the relationship of S-parameter and input impedance, and the condition of transmission zeros and transmission poles of the bandpass filter, it can be calculated that in a frequency range of $2f_0$, three transmission zeros can be obtained, which can be formulated respectively as

$$f_{TZ1} = \frac{8f_0}{3\pi}arctan\sqrt{\frac{1}{2K+1}} \tag{4}$$

$$f_{TZ2} = \frac{3f_0}{2\pi}arctan\sqrt{k_1} \tag{5}$$

$$f_{TZ3} = 2f_0 - \frac{8f_0}{3\pi}arctan\sqrt{\frac{1}{2K+1}} \tag{6}$$

Here f_0 is the filter working frequency. It is noted from (4)-(6) that the first and the third transmission zeros are controlled by the open-circuited SIRs, while the second transmission zero is controlled by the coupled line terminal loading multi-mode resonator.

The transmission poles can be formulated respectively as

$$f_{TP1} = \frac{8f_0}{\pi}arctan\sqrt{k_1} - 2f_0 \tag{7}$$

$$f_{TP2} = \frac{8f_0}{\pi}arctan\sqrt{k_2} \tag{8}$$

$$f_{TP3} = 2f_0 - \frac{8f_0}{\pi}arctan\sqrt{k_2} \tag{9}$$

$$f_{TP4} = 4f_0 - \frac{8f_0}{\pi}arctan\sqrt{k_1} \tag{10}$$

with $k_1 = (3Z_c + 2Z_r + 2\sqrt{2Z_c^2 + 2Z_cZ_r + Z_r^2})/(Z_c + 4Z_r)$, and $k_2 = (3Z_c + 2Z_r - 2\sqrt{2Z_c^2 + 2Z_cZ_r + Z_r^2})/(Z_c + 4Z_r)$.

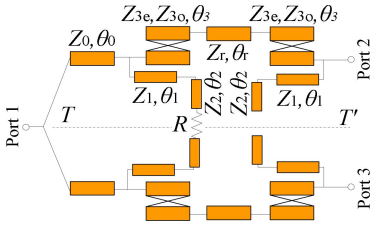

Fig. 6. Transmission line circuit scheme of the wideband FPD.

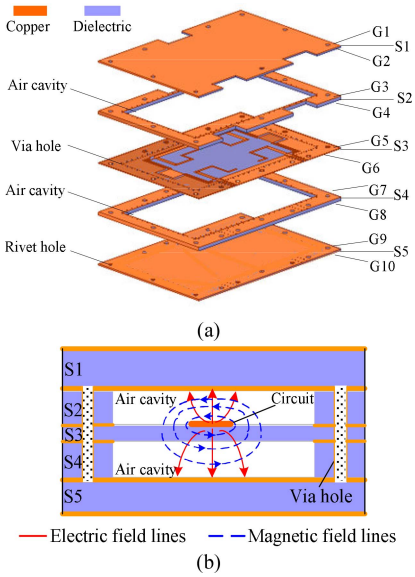

Fig. 7. Total circuit structure of the wideband FPD. (a) 3-dimensional view of each substrate. (b) Cross section view and the circuit electromagnetic field.

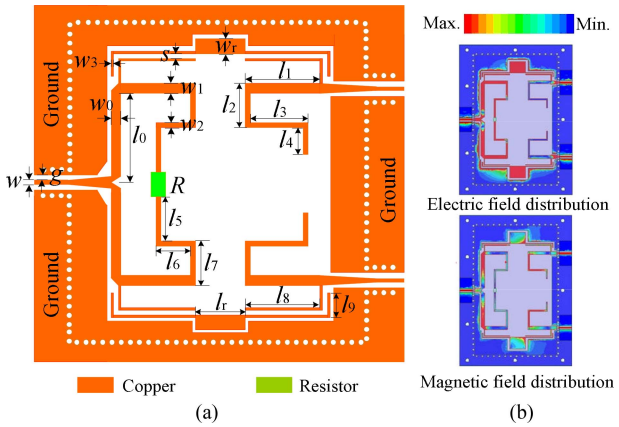

Fig. 8. Core circuit and electromagnetic field distributions. (a) Core circuit structure. (b) Simulated electric/magnetic field distributions.

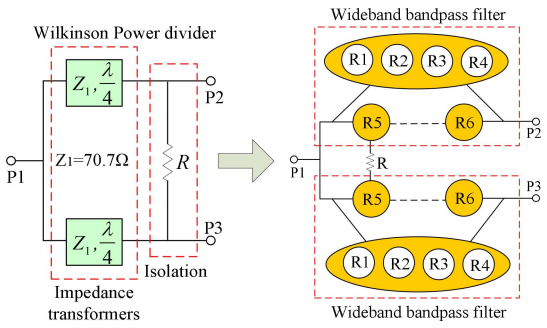

Fig. 9. Coupling structure of the proposed wideband FPD.

B. Filtering Power Divider Implementation

The transmission line circuit model of the wideband FPD is schemed based on the multi-mode bandpass filter and a Wilkinson power divider, as is plotted in Fig. 6, where the multi-mode bandpass filter is used to replace the impedance transformer, and an isolation resistor R is bridge-connected between the first stage SIRs. The circuit is symmetrical along TT'. According to the multi-mode resonator bandpass filter, the SISL technique, and the transmission line circuit model as shown in Fig. 6, a self-packaged multi-layer suspended wideband FPD has been constructed, as is shown in Fig. 7, where the 3-dimensional (3D) circuit structure is shown in Fig. 7(a), and the circuit cross-section view is shown in Fig. 7(b). The circuit is implemented by five substrates labeled by S_1 to S_5 with ten faces labeled by G_1 to G_{10}, where S_2 and S_4 have etched air cavities, and the electromagnetic field concentrates in the cavities, S_3 is the core circuit layer, and the circuit is packaged by S_1 and S_5. The PCB cut air cavities not only reduce the dielectric loss and implement suspension, but also make the required tri-dimensional elements such as resistors set down in the cavity conveniently. The circuit feeding is conductor-backed coplanar waveguide (CBCPW) structure, and there is a transition between the CBCPW and the suspended line. Via holes which are around the air cavities are used not only for the undesired harmonics suppression, but also for minimizing the electromagnetic waves leakage. Via holes cut-through S_2, S_3 and S_4. Each substrate can be designed and fabricated individually, and then be bounded by rivets. S_1, S_2, S_4 and S_5 are FR-4 material, which have a dielectric constant of 4.4, and a thickness of 0.6mm, 1.4mm, 1.4mm and 0.6mm, respectively. S_3 is designed on Rogers RT/duroid 5880 substrate with a dielectric constant of 2.2 and a thickness of 0.254mm. The using of hybrid substrates is because that FR-4 is more rigid, which is more suitable for packaging, while Rogers RT/duroid 5880 has less loss tangent, which is better for core circuit design.

The core circuit is implemented according to the transmission line circuit scheme, as is shown in Fig. 8(a). When designed working at 3.8GHz with a fractional bandwidth (FBW) of 61.5%, a passband insertion loss of no more than 0.4dB, a return loss of no less than 18dB, and an isolation of no less than 20dB within 8GHz, the dimensions of the wideband FPD can be obtained by the transmission line theory and the circuit specifications as $w = 0.8$, $w_0 = 2$, $w_1 = 1.8$, $w_2 = 0.8$, $w_3 = 0.4$, $w_r = 6.5$, $l_0 = 21.6$, $l_1 = 11.1$, $l_2 = 10.8$, $l_3 = 9.52$, $l_4 = 4.32$, $l_r = 8.3$, $l_5 = 9.8$, $l_6 = 6.2$, $l_7 = 10.8$, $l_8 = 13.1$, $l_9 = 3.7$, and s=0.5, unit: mm. $R = 225\Omega$, and the center distance between neighboring via holes is 3mm. Simulated electric/magnetic field distributions are plotted in Fig. 8(b), it is seen that the circuit electromagnetic field dominantly concentrates on the coupled-line terminal loading multi-mode resonator and the SIRs neighboring the input port. Coupling structure of the proposed wideband FPD is plotted in Fig. 9, where R1, R2, R3 and R4 represent the multi-mode resonator, while R5 and R6 represent the folded SIRs.

Parameters of the transmission line circuit in Fig. 6 can be obtained as $Z_0 = 26.65\Omega$, $\theta_0 = 129.55°$, $Z_1 = 28.98\Omega$, $\theta_1 = 77.02°$, $Z_2 = 52.36\Omega$, $\theta_2 = 153°$, $Z_r = 9.64\Omega$, $\theta_r = 50.93°$, $Z_{3e} = 85.55\Omega$, $Z_{3o} = 73.06\Omega$, and $\theta_3 = 95.42°$,

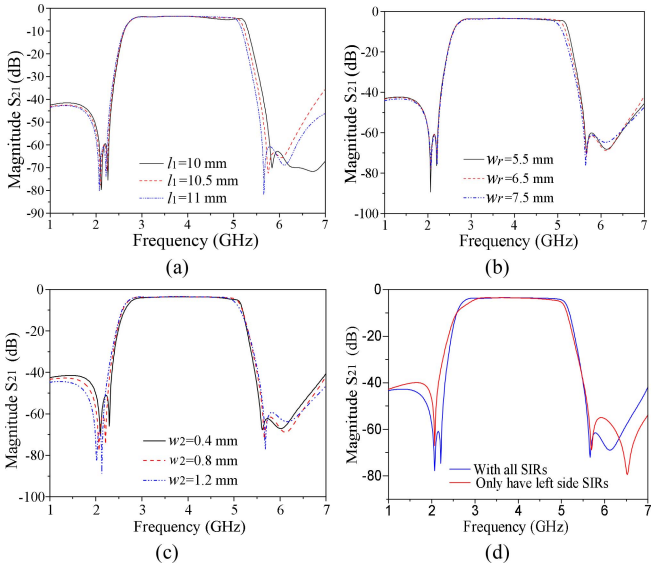

Fig. 10. Simulated S_{21} variations versus some physical parameters. (a) S_{21} variations versus l_1. (b) S_{21} variations versus w_r. (c) S_{21} variations versus w_2. (d) S_{21} variations with all SIRs and part SIRs.

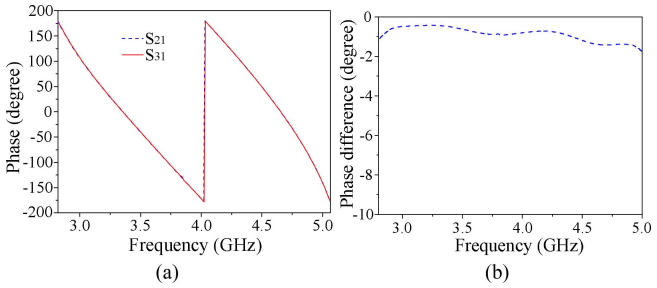

Fig. 11. Simulated circuit phase and phase imbalance in transmission paths 1-2 and 1-3. (a) Circuit phase of S_{21} and S_{31}. (b) Phase difference between two transmission paths within the passband.

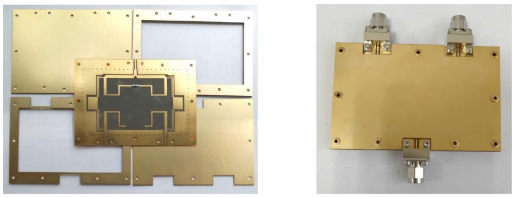

Fig. 12. Photograph of the fabricated hardware. (a) Fabricated each substrate. (b) Assembled whole circuit.

where Z_i is the characteristic impedance corresponding to the physical parameter w_i, $i = 0, 1, 2, r$. θ_0 and θ_1 are the electric lengths corresponding to the physical lengths of l_0 and l_1, respectively. θ_2 is the electric length corresponding to the physical length of $l_5 + l_6 + l_7$. Z_{e3} and Z_{o3} are the characteristic impedances of the even/odd-mode of the coupled-line, respectively, while θ_3 is the electric length of the coupled-line. For the obtained electric parameters, it can be calculated that three transmission zeros locating at 1.95/2.03/5.65GHz are achieved according to formulas (4)-(6), while transmission poles of 3.21/3.69/3.91/4.68GHz are achieved according to formulas (7)-(10).

Simulated S_{21} of the proposed FPD versus physical parameters l_1, w_r and w_2 are plotted in Figs. 10(a), (b), and (c), respectively. It can be seen that 1) FPD bandwidth can be adjusted/controlled by l_1, as shown in Fig. 10(a), which is because that the weak coupling of R5 and R6 can be changed with l_1 increasing, while FPD bandwidth is related with the electromagnetic coupling. 2) FPD bandwidth increases with w_r decreasing, as is shown in Fig. 10(b), which is because that wideband performance is dominantly determined by the multi-mode resonator, and decreased w_r makes some of the resonance distance between f_{ev1}, f_{od1}, f_{ev2} and f_{od2} become wider, namely decreased w_r introduces bigger f_{od2}–f_{ev1}. In the research, we also noted that FPD bandwidth increases with coupled-line width w_3 increasing. 3) FPD transmission zeros can be adjusted by w_2, and TZs are more close to center frequency with w_2 decreasing, as is seen in Fig. 10(c), of course, TZs also can be adjusted by w_1. 4) FPD transmission zeros not only can be adjusted by w_1/w_2, namely impedance ratio of SIR, but also by the quantity of SIRs, as is shown in Fig. 10(d), and it indicates that when there are only left-hand SIRs, the TZs at lower stopband change from two to one, and this transmission zero keeps away from the center frequency, while the out-of-band rejection and passband flatness get worse compared with the case of with all SIRs. It can be concluded that bandwidth and TZs of the proposed FPD can be adjusted/controlled.

Simulated circuit phase and phase difference in transmission paths 1-2 and 1-3 within FPD passband are plotted in Figs. 11(a) and (b), respectively, which indicates that the proposed FPD has a phase imbalance of no more than 1.4°.

III. Experimental Results

The proposed wideband FPD has been fabricated by using FR-4 and Rogers RT/duroid 5880 substrates with dielectric constants of 4.4 and 2.2, respectively, the substrate thickness from S_1 to S_5 are 0.6mm, 1.4mm, 0.254mm, 1.4mm and 0.6mm, respectively. The fabrication photographs are shown in Fig. 12, where the fabricated individual substrate is shown in Fig. 12(a), and the assembled whole circuit is shown in Fig. 12(b). The measurement is performed by Agilent E5071C vector network analyzer, and the measured results are illustrated in Figs. 13(a), (b), and (c). It is seen from the measurements that the proposed FPD centers at 3.9GHz with a fractional bandwidth of 63.6%, an in-band insertion loss of no more than 0.74dB (the fixed 3dB insertion loss of the power divider is subtracted), a return loss of no less than 14.6dB, and a out-of-band rejection of more than 40dB, while three TZs at 2.04GHz, 2.25GHz and 5.64GHz with S_{21} attenuation of more than 57dB have been implemented, as shown in Fig. 13(a). The measured TZs are close to the prediction of 2.1GHz, 2.2GHz and 5.5GHz. It is also seen that the measured S_{22}/S_{33} has an attenuation of no less than 13.6dB, while the measured in-band isolation (S_{23}) is no less than 18.3dB, and the out-of-band isolation is more than 36.58dB, as have been demonstrated in Fig. 13(b). The simulated and measured group delay is plotted in Fig. 13(c), and it is seen that the measured group delay in the passband is relative flat, which has a variation of no more than 0.5ns from 2.8-5.0GHz. The measurement approaches to the predictions, and the wide passband, high frequency selectivity as well as the high out-of-band rejection have been demonstrated. The discrepancy between the measurement and the prediction is due to the fabrication uncertainty, material error and the system error in test.

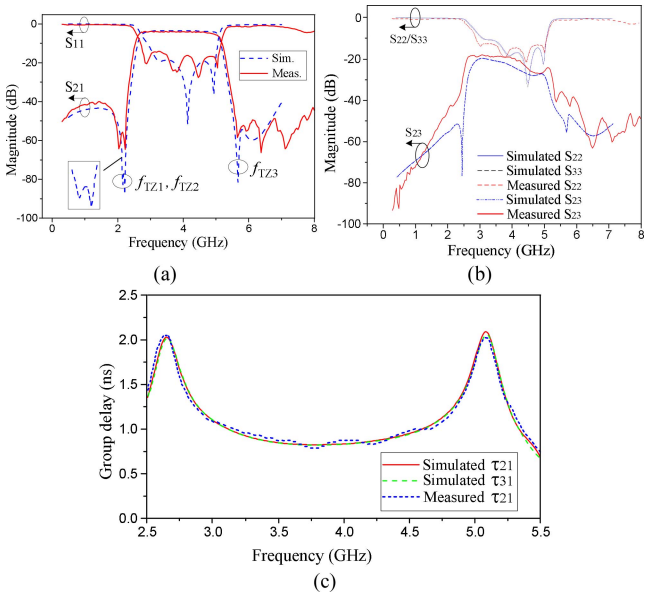

Fig. 13. Measurement and simulation comparison. (a) Comparison of the measured and simulated S_{11}/S_{21}. (b) Comparison of the measured and simulated $S_{23}/S_{22}/S_{33}$. (c) Comparison of the measured and simulated τ_{21}/τ_{31}.

TABLE I
COMPARISON OF THIS BRIEF AND THE RELATED REPORTS

Ref.	CT/f_0	FBW (%)	IL (dB)	IBI (dB)	TZs /Rs	OS (dB)	SP	Size (λg×λg)
[7]	M/3.0	62	0.6	16.5	2/2	>29	no	-
[8]	M/1.99	43.7	0.74	20	2/3	>28	no	0.33×0.25
[9]	M/2.5	78	0.7	17.5	2/1	>16	no	0.74×0.31
[10]	M/3.0	66	-	18.5	0/3	>40	no	0.56×0.18
[11]	M/2.35	55.3	3.59	20	1/2	>20	no	0.27×0.36
[12]	M/2.42	100	1.1	15	2/3	>35	no	0.2×0.32
ours	SISL/ 3.9	63.6	0.74	18.3	3/1	>40	yes	0.29×0.47

Ref.-reference, CT-Circuit type, M-microstrip, f_0-center frequency (GHz), IL-insertion loss, IBI-In-band isolation, TZs-transmission zeros, Rs-isolation resistors, SP-Self-packaging, OS-out-of-band suppression.

Experimental results comparison of the proposed FPD and the related reports is listed in Table I. It can be seen that the proposed work not only has new suspended and self-packaged structure, but also has more transmission zeros, more out-of-band suppression, and fewer isolation resistor. Compared with some related works, features of wideband, low loss, high frequency selectivity and high out-of-band rejection have been demonstrated.

IV. CONCLUSION

A multi-mode wideband filtering power divider which centers at 3.9GHz with three transmission zeros by using multi-mode and self-packaged SISL technologies is proposed, and advantages of high frequency selectivity, low passband insertion loss and high out-of-band rejection have been demonstrated by experiment. In our research, it is noted that the suspended FPD has better passband IL and better out-of-band rejection compared with the planar FPD. The proposed FPD brings a feasible case of circuit integration by a suspended multi-layer structure with common PCB technique, and some other elements/circuits can be easily added/integrated in the air cavities, meanwhile, more complicated integration circuit can be realized by adding more layers with vertical connection.

REFERENCES

[1] Q. Li, Y. Zhang, and C.-T. M. Wu, "High-selectivity and miniaturized filtering wilkinson power dividers integrated with multimode resonators," *IEEE Trans. Compon. Packag. Manuf. Technol.*, vol. 7, no. 12, pp. 1990–1997, Dec. 2017.

[2] J. Shao, S. Huang, and Y. Pang, "Wilkinson power divider incorporating quasi-elliptic filters for improved out-of-band rejection," *Electron. Lett.*, vol. 47, no. 23, pp. 1288–1289, Nov. 2011.

[3] B. Lee, S. Nam, and J. Lee, "Optimization-free design equations for narrowband equal-division filtering power divider with pre-specified filtering response and wideband isolation," *IEEE Trans. Circuits Syst. I, Reg. Papers*, vol. 66, no. 7, pp. 2496–2507, Jul. 2019.

[4] X. Zhang, K. Wang, and B. Hu, "Compact filtering power divider with enhanced second-harmonic suppression," *IEEE Microw. Compon. Lett.*, vol. 23, no. 9, pp. 483–485, Sep. 2013.

[5] X.-L. Zhao, L. Gao, X. Y. Zhang, and J.-X. Xu, "Novel filtering power divider with wide stopband using discriminating coupling," *IEEE Microw. Compon. Lett.*, vol. 26, no. 8, pp. 580–582, Aug. 2016.

[6] Y.-L. Lu, Y. Wang, C. Hua, and T. Liu, "Wide stopband out-of-phase filtering power divider using double-sided parallel-strip line," *Electron. Lett.*, vol. 53, no. 25, pp. 1659–1661, Dec. 2017.

[7] X. Yu and S. Sun, "A novel wideband filtering power divider with embedding three-line coupled structures," *IEEE Access*, vol. 6, pp. 41280–41290, 2018.

[8] Y. Wang, F. Xiao, Y. Cao, Y. Zhang, and X. Tang, "Novel wideband microstrip filtering power divider using multiple resistors for port isolation," *IEEE Access*, vol.7, pp. 61868–61873, 2019.

[9] Y. Liu, L. Zhu, and S. Sun, "Proposal and design of a power divider with wideband power division and port-to-port isolation: A new topology," *IEEE Trans. Microw. Theory Techn.*, vol. 68, no. 4, pp. 1431–1438, Apr. 2020.

[10] C. Bao, X. Wang, Z. Ma, C. Chen, and G. Lu, "An optimization algorithm in ultrawideband bandpass wilkinson power divider for controllable equal-ripple level," *IEEE Microw. Compon. Lett.*, vol. 30, no. 9, pp. 861–864, Sep. 2020, doi: 10.1109/LMWC.2020.3011516.

[11] H. Hao and X. Ni, "Wideband filtering power divider with wide rejection bandwidth and isolation," *Electron. Lett.*, vol. 55, no. 7, pp. 395–396, Apr. 2019.

[12] K.-D. Xu, Y. Bai, and D. Li, "Wideband four-way filtering power divider using simple three-line coupled structures," in *Proc. IEEE MTT-S Int. Wireless Symp. (IWS)*, Guangzhou, China, May, 2019.

[13] X. Wang, J. Wang, W.-W. Choi, L. Yang, and W. Wu, "Dual-wideband filtering power divider based On coupled stepped-impedance resonators," *IEEE Microw. Compon. Lett.*, vol. 28, no. 10, pp. 873–875, Oct. 2018.

[14] G. Zhang, X. Wang, and J. Yang, "Dual-band microstrip filtering power divider based on one single multimode resonator," *IEEE Microw. Compon. Lett.*, vol. 28, no. 10, pp. 891–893, Oct. 2018.

[15] W. Menzel and A. Belalem, "Quasi-lumped suspended stripline filters and diplexers," *IEEE Trans. Microw. Theory Techn.*, vol. 53, no. 10, pp. 3230–3237, Oct. 2005.

[16] I. Angelov, A. Spasov, I. Stanchev, and L. Urshev, "19 GHz suspended-line FET amplifier," in *Proc. 12th Eur. Microw. Conf.*, 1982, pp. 133–137.

[17] O. Palamutcuoglu and I. Kurhan, "Broadband microwave mixer mounted on suspended line baluns," *Proc. 7th Mediterr. Electrotech. Conf.*, 1994, vol. 2, pp. 500–503.

[18] I.-H. Kang, Y.-G. Kim, D.-S.Woo, S.-K. Kim, and K.W. Kim, "Design of a tunable oscillator using a suspended-stripline resonator," in *Proc. 7th Eur. Microw. Integr. Circuits Conf. (EuMIC)*, Oct. 2012, pp. 762–765.

[19] K. Ma and K. T. Chan, "Quasi-planar circuits with air cavities," PCT Patent WO/2007/149046.